Modelling metastatic melanoma in zebrafish

Groenewoud, A.

Chapter 5:

Melanin promotes melanoma metastasis by inhibiting ferroptosis

Chapter 5: Melanin promotes melanoma metastasis by inhibiting ferroptosis

Arwin Groenewoud[1, *], Maria Chiara Gelmi[2, *], Jie Yin[1], Gerda E. M. Lamers[1], Martine J. Jager[2], B.E Snaar-Jagalska[*]

1) Institute of Biology, Leiden University, Leiden, The Netherlands

2) Department of Ophthalmology, Leiden University Medical Center, Leiden, The Netherlands

*) These authors contributed equally

*Corresponding author: Prof Dr B.E. Snaar-Jagalska, Institute of Biology, PO Box 9502, Leiden University, Leiden, The Netherlands

E Mail: b.e.snaar-jagalska@biology.leidenuniv.nl

Manuscript in preparation

Abstract

Death in melanoma patients is mainly caused by metastasis. Increased melanin levels in cutaneous melanoma are associated with decreased patient survival. However, the role of melanin in this process remains poorly understood. Here, we show that melanin protects circulating melanoma cells from ferroptosis increasing their metastatic potential. We describe a strong association of high expression of the melanin biosynthesis gene *TYRP1,* the lipid peroxide reducer GPX4 and ferroptosis related mitochondrial voltage dependent anion channel 1 (VDAC1) with reduced melanoma specific survival. Furthermore, melanin levels in primary uveal melanoma patient cells positively correlate with their metastatic potential in zebrafish. Modulation of melanin levels in uveal, cutaneous and conjunctival melanoma cells results in enhanced or reduced metastatic potential upon increased or decreased melanin levels, respectively. Finally, melanin depletion sensitizes melanoma cells to ferroptosis inducers in zebrafish leading to a decreased metastatic burden. Collectively, our data identify melanin biosynthetic enzymes as potential future target to treat melanoma.

Introduction

Melanoma is one of the most common malignancies, and arises from melanocytes following malignant transformation. Subsequent metastatic spread, and not the growth of the primary tumor, kills up to 90% of cancer patients[1,2,3]. For intra-ocular melanoma, it is assumed that only a small fraction of cells that escape from the primary tumor successfully establish a metastatic colony, indicating a strong selective pressure on disseminating cancer cells within the circulation[4–6]. Among the key factors in curbing metastatic dissemination in the circulation are reactive oxygen species (ROS)[7,8]. These ROS are derived from either intracellular or extracellular stressors[9–12]. In healthy skin, melanin functions to protect against Ultraviolet (UV) radiation by preventing direct DNA damage (UV-B) and ROS-mediated genotoxicity (UV-A)[13–15]. We propose that melanin protects transformed melanocytes in a similar manner, thus enhancing cell survival during dissemination and the metastatic potential of melanoma cells.

Melanomas are derived from neuroectodermal progenitor cells during embryonic development, giving rise to different populations of melanocytic precursors[16,17]. All melanocytes harbor intrinsic melanogenic potential, which is normally induced in the skin in a UV-dependent manner through the αMSH-MITF-TYR axis[16,18]. In ocular melanocytes, melanin biosynthesis is induced through a largely unknown mechanism[18–20].

In contrast, most melanoma cell lines derived from melanated lesions lose their capacity to synthesize melanin *in vitro*. Conversely, patient-derived xenograft models retain their melanogenic potential, underscoring the apparent selective pressure *in vivo*. Interestingly, studies suggest an inverse correlation between pigmentation and migratory capacity[21,22]. Strikingly, the *in vivo* cutaneous melanoma model described by Pinner et al shows an enhancement of distant metastasis in the presence of heightened melanin levels[22].

One of the possible mechanisms of ROS-mediated cell death is thought to be ferroptosis, a lipid peroxidation-based, iron-dependent mechanism of cell death[23–26]. Ferroptosis seems to be more strongly induced in cutaneous melanoma (CM) cells expressing oncogenic RAS variants, possibly due to an increase in cellular iron levels[23,26,27].

During ferroptosis, either induction of mitochondrial stress, endoplasmic reticulum stress through inhibition of voltage-gated anion channel, or inhibition of the cysteine/glutamate antiporter system (System Xc-) cause a dramatic increase of intracellular ROS. This sharp increase in ROS catalyzes lipid peroxidation and is presumed to lead to subsequent cell membrane permeation and cell death, while maintaining nuclear integrity[28,29].

Glutathione peroxidase 4 (*GPX4*) functions as a lipid peroxide reducer, effectively reverting the damage done by ferroptosis[24,25]. Intracellular glutathione is used as a reservoir of ROS reduction and can effectively curb ferroptotic cell death. Common inducers of ferroptosis either interfere with mitochondrial or electron transport chain functions, the cellular system Xc- (erastin), or inhibit GPX4[30].

We observed a positive correlation between melanin inclusion in primary UM tissues and their respective engraftment capacity in a zebrafish model. We propose that the retained melanin protects melanoma cells in the circulation, by alleviating ferroptosis and its related intracellular ROS-mediated damage, thereby enhancing the metastatic potential of melanoma cells.

To address this hypothesis, we have tested a set of different melanoma cell lines from CM and conjunctival melanoma (CoM) origin with melanated and non-melanated phenotypes. We used a melanin depletion strategy for CM and CoM cell lines. Conversely, we developed a biological melanin transfer system, allowing us to re-introduce melanin from a melanated CM donor cell line to non-melanated uveal melanoma (UM) cell lines.

We correlated melanin inclusion within UM, CM, and CoM with an enhanced metastatic potential and proved that depletion of melanin in melanated melanoma cells decreases their metastatic potential. Furthermore, we showed that transfer of extraneous melanin into UM cells confers protection to stress during hematogenous dissemination. Finally, we demonstrated that melanin depletion significantly enhances cellular susceptibility to ferroptotic insult during dissemination *in vivo*. In conclusion, we confirmed that melanin can act as a pro-metastatic factor protecting cells from ROS and demonstrated the importance of melanin in blocking ferroptosis during metastatic dissemination.

Materials and methods:

Uveal melanoma

UM tissue was obtained from patients from the Leiden University Medical Center (LUMC) in Leiden, The Netherlands. Part of the tumor was snap frozen with 2-methyl butane and used for DNA and RNA isolation, while the remaining tumor tissue was fixed in 4% neutral-buffered formalin and embedded in paraffin.

For a gene expression array, material was obtained from 64 patients who underwent an enucleation for UM between 1999 and 2008, of which 51% were male and 49% female. The mean age at the time of enucleation was 61 years. The mean follow-up time (defined as the time period between enucleation and death) was 83 months (range 2 to 229 months). Follow-up was updated in 2020. At the end of follow up, 17 (27%) patients were alive, 37 (58%) patients had died because of metastasis, four (6%) had died because of other causes and six (9%) had died but the cause of death was unknown. Gene expression was determined with the Illumina HT12v4 array (Illumina, Inc., San Diego, CA, US). As published by de Lange et al 2015[39].

Fresh tumor material was obtained directly after enucleation to establish spheroids.

We also assessed mRNA levels of tumors included in the TCGA database (n=80) as published by Robertson et al 2017[40–42].

Institutional Review Board Statement

The analysis was approved by the METC of the LUMC (B14.003/SH/sh Approval Biobank OOG-2 “Oogtumoren (of een verdenking hierop)”, protocol Uveamelanoom-lab B20.026, approval June 2020). Fresh material was used for spheroids under METC protocol UM CURE 2020: Prospective collection: new treatment options for metastatic uveal melanoma (NL57166.058.16). The research adhered to Dutch law and the tenets of the Declaration of Helsinki (World Medical Association of Declaration 2013; ethical principles for medical research involving human subjects). Each patient had signed an informed consent.

Stable cell culture

Cell line SK-Mel28 was acquired from ATCC, while other cell lines were kindly provided by Dr. B Rinner (Mugmel2)[31], Prof. Dr. M.J. Jager (CRMM1 and CRMM2)[43], Dr. A.G Jochemsen (OMM2.3)[44] and Dr S. Alsafadi (XMM66)[45]. Human CM PDX derived cell lines PDX11917 (alternatively named, M011-5.X1.CL) was kindly provided by Prof. D. Peeper[34].

We routinely imaged or assessed the cells used in this project using an inverted automated EVOS microscope (Thermo scientific, Waltham, USA) using eGPF and RFP filters to ensure retention of normal phenotypes and to verify fluorescent tracer expression

Cells were cultured in a humidified incubator, 5% CO_2 at 37°C, all cells were intermittently tested for the absence of mycoplasma using the universal mycoplasma detection Kit (American type cell culture (ATCC), LGC Standards GmbH, Wesel, Germany) according to the manufacturer's prescriptions. All cells, with the exception of primary UM cells, were cultured in Dulbecco's modified eagles' medium (DMEM), enhancing melanin biosynthesis due to its high tyrosine levels (3,5-fold higher than RPMI1640). DMEM was supplemented with 10% fetal bovine serum and glutamax (GIBCO, Thermo scientific). Cells were propagated through subsequent medium removal, washing with Dulbecco's phosphate buffered saline (DPBS) and incubation with 2mL tryplE (GIBCO). Cells were carefully dispersed after the addition of DMEM up to the original culture volume.

Chemical melanin depletion

Commonly phenylthiourea (PTU, Sigma) is used, dissolved in water, for the inhibition of melanation of zebrafish larvae. We reasoned that PTU could also be used to block the biosynthesis of melanin *in vitro*. To this end, we treated mugmel2 cells with a concentration range of 1 - 0.0625 mM, dissolved in dimethylsulfoxide (DMSO, Sigma).

Ethics statements

All animal experiments were approved by Animal Experiments Committee (Dier Experimenten Commissie, D.E.C.) under license AVD1060020172410. All animal were maintained in accordance with local guidelines using standard protocols (www.ZFIN.org)

Zebrafish engraftment

Primary cells were dispersed as described previously by Groenewoud et al[46]. In brief, cells were harvested from adherent cultures through tryplE addition, and subsequently concentrated by centrifugation. Cells were transferred to a 15 mL centrifuge tube and centrifuged for 5 minutes at 200 x g, followed by complete removal of all DPBS. The cell pellet was resuspended in 1 mL DPBS and subsequently counted. The cells were pelleted again at 200 x g whereafter the DPBS was removed after centrifugation. To completely remove all DPBS the cells were centrifuged for another minute at 200 x g, the cell pellet was resuspended to a final concentration of $250 \times 10^6 \cdot mL^{-1}$ in 2% polyvinylpyrrolidone 40 (PVP_{40}) in DPBS.

In brief, cells were injected into zebrafish larvae of either *casper* or *Tg(fli:eGFP x casper)* zebrafish larvae at 48hpf into the duct of Cuvier (doC) also known as the embryonic common cardinal vein using a capillary glass needle.

Chemical compounds and drugs

Erastin, RSL3 and mitomycin-C were purchased from Cayman chemical (Ann Arbor, Michigan, USA). PTU was purchased from Sigma (Sigma, Zwijndrecht, the Netherlands)

Drug treatment of engrafted zebrafish

Fish were bred and maintained until 48hpf, whereafter they were injected with approximately 300-400 cells per individual, through the doC allowing the cells to disseminate hematogenously within several hours after injection. One hour post injection possible dead larvae were removed from the injected pool and the injected individuals were divided over clean Petri dishes, with approximately 100-150 individuals per dish. Approximately 16hpi the injected larvae were screened using a stereo epi-fluorescent microscope, all the unwanted phenotypes (uninjected, malformed) were discarded. All larvae were randomly assigned to experimental groups in a 24 wells plate, with at least 6 wells containing 6 fish per well per condition. After plating the fish, approximately 16-18hpi the fish were treated with the appropriate level of inhibitor dissolved in DMSO and diluted to the final concentration in eggwater.

Data acquisition and analysis

For kinetic measurements of tumorigenicity engrafted individuals were imaged at 1,4- and 6-days post implantation using an epifluorescent stereo microscope. At the first time point the microscope settings (exposure time and gain) were set on the control group of each sample population, taking care that signal saturation was not attained to allow for signal increase due to cell growth. Each sample set was imaged using the same settings throughout the duration of the experiment. All images were analyze using a custom imageJ MACRO (Zenodo DOI: 10.5281/zenodo.4290225). Data was normalized to the vehicle control group of each experimental population; two biological replicates were combined with at least 20 individuals per biological replicates.

Transmission electron microscopy sample preparation

Cells were cultured on thermanox (Thermo scientific/Nunc) coverslips, fixation was performed with a mixture of 2% glutaraldehyde and 2% formaldehyde in 0,1M Na-cacodylate buffer pH=7.2

Post-fixation was performed with 1% OsO_4 +$K_4Fe(CN)_6$ (15µg/ml) in demineralized water for 1 hour at room temperature, after dehydration through a graded series of ethanol, all specimens were kept for 16 hours in epoxy resin (Agar Scientific,) before embedding. Ultrathin sections were collected on formvar-coated one hole copper grids. Electron microscopy images were obtained with a JEOL 1400Plus Transmission Electron Microscope (Tokyo, Japan) at 80KV.

WST1 proliferation assay

Mugmel2 cells (7,5 × 10^4) were seeded in 100 µL in flat bottom 96 wells plates (Corning), combining both cells with prior chemical inhibition of melanin biosynthesis and vehicle control (DMSO) treated cells in the same plate, in triplicate. Cell were left to attach overnight and were subjected to ferroptosis induction using erastin and RSL3, compared to DMSO control for 3 days. Proliferation was measured based on WST1 conversion, following the manufacturers description. Values were normalized to vehicle treated control, 100% survival, and plotted.

qPCR analysis

Cells were harvested ($1x10^6$) by centrifugation (200 x g for 5 min at 25°C. Whole RNA was isolated using the Qiagen RNeasy kit (Qiagen) according to the manufacturer's description, treating the isolate on-column with RNase free DNAse for 15 minutes at room temperature. Total RNA yield was quantified using Nanodrop 2000 (Thermo scientific, Wilmington, USA) and 1 µg RNA was used to synthesize cDNA using the iSCRIPT cDNA kit (Biorad, Hercules, USA) according the manufacturers description.

Detection was performed using the iQ5 QPCR apparatus (Biorad), using IQ green super mix (Biorad), for 35 cycles. Primers were diluted in PCR grade nuclease free water (Gibco) at a concentration of 100 µM. All primers were tested for, and passed an efficiency test prior to use and were used at a final concentration of 10 pmol.

Glyceraldehyde-3-phosphate dehydrogenase (GAPDH) expression level was used as an internal reference for each experimental primer set. Transcript levels were corrected for loading to GAPDH expression and normalized using the ΔCT method. All samples were measured in at least 3 biological triplicates.

Cellular ROS Assay reactive oxygen measurement

To measure overall intracellular ROS concentrations, and the influence of intracellular melanin on ROS induction on mugmel2(-eGFP cells), we seeded $7,5 \times 10^4$ cells in 100µL per well, in black skirted glass bottom 96 wells plates (Corning). The cells were allowed to adhere for 16 hours prior to analysis. In the same plate we seeded mugmel2 cells with and without prior melanin depletion, in triplicate, in DMEM, without phenol red. ROS inducers were added, diluted in phenol red free culture medium, to a final concentration of 500, 100, 500 µM Paraquat, Menadione and hydrogen peroxide (H_2O_2) in 50 µL, respectively. After addition of ROS inducers, the cells were incubated for 30 minutes. Subsequently, red fluorescent Cellular ROS reagent (Abcam, Cambridge, United Kingdom) was added, 50 µL diluted in phenol red free DMEM to a 2x concentration. Cells were treated for 30 minus followed with 2 washes with PBS and subsequent fixation with 4% PFA at room temperature for 10 minutes. Cells were washed with PBS containing 200 mM glycine, 0.1 µg/mL and 4',6-Diamidine-2'-phenylindole dihydrochloride (DAPI) for 1 hour at 4 °C. Plates were imaged using an EVOS M7000 microscope (Thermo Fischer Scientific, Darmstadt, Germany), imaging DAPI stained nuclei, green cells outline, red ROS reagent and brightfield at 20x

magnification. Data was analyzed using ImageJ, measuring ROS reagent signal intensity in GFP positive area, while normalizing for the number of cells (DAPI positive nuclei counts).

Melanin measurement

Melanin was measured spectrophotometrically, after solubilization in 1M NaOH, containing 10% DMSO (v/v) as described by Friedman et al.[18] In brief, cell pellets were collected of 2 × 10^6 cells by tryplE incubation, inactivation and subsequent centrifugation. Cells were frozen at -20°C prior to measurement. A standard curve of chemical eumelanin (Sigma, Zwijndrecht, the Netherlands) was made ranging from 1 mg/mL to 7,8125 µg/mL (2-fold dilution series) in triplicate. Standards and samples were solubilized by addition of 1M NaOH, 10% DMSO and incubation at 80°C for 30min. melanin negative samples (MDA-mb231 cells expressing the same reporter gene were used as a negative control) were taken along and were used to subtract backgrounds after measurement. Absorbance was measured at 420nm and plotted; concentration was inferred from the standard curve.

Co-culture experiments

For the melanin transfer co-culture experiments we cultured highly melanotic cell line mugmel2[31] expressing eGFP in the absence and presence of phenylthiourea (PTU) a generic inhibitor of melanin biosynthesis.[20,47] After two passages the PTU treated cells were considered melanin depleted, where depletion was validated through the spectrophotometric measurement previously described. The cells were treated with 100 µg/mL mitomycin-C (Sigma) in culture medium, under normal culture conditions, for three hours. The cells were washed with sterile PBS and DMEM subsequently prior to harvesting. UM cells were harvested as previously described. For both UM-tdTOM lines 1 × 10^6 cells were seeded in a 75 cm^2 culture flask mixed together with melanin depleted cells (mel^-) and with highly melanated cells (mel^+), the cells were cultured for 4 days at normal culture conditions. Prior to harvesting the cells were checked for presence of remnant eGFP signal (donor cells) and tdTOM (acceptor cells) and for presumptive melanin transfer. The cells were washed extensively, prior to harvesting as previously described.

Lentiviral over expression and shRNA construct generation

Lentiviral overexpression and shRNA constructs from the Sigma TRC mission library were kindly provided to us by Dr. M. Rabelink from the department of department of molecular cell biology, from the Leiden university medical center (Constructs detailed in supplementary table ST1). Lentiviral particles were generated as described previously by Heitzer er al 2019[33]. In brief Hek293T cells were grown to 80-90% confluency and transfected after a medium change with psPAX2, pMD2.G and the transfer plasmid of choice at a respective molar ratio of 1.3 pmol, 0.72 pmol, 1.64 pmol using 30uL lipoD293 on a 75cm2 culture flask. Cell culture medium was exchanged for 20mL complete DMEM 24 hours post transfection. Viral particles were harvested 72h after the original transfection.

Patient data analysis

LUMC cohort: Genetic information on TYR, TYRP1 and DCT and information on the chromosome 3 status and BAP1 status was obtained from a database of 64 UMs in eyes enucleated at the Leiden University Medical Center between 1999 and 2008.

TCGA cohort: Information for both uveal and cutaneous melanoma patients were gathered from The Cancer Genome Atlas (TCGA), which is a publicly available database available at https://www.cancer.gov/tcga. The TCGA database for UM contains 80 patients and the TCGA database for cutaneous melanoma contains 458 patients. Data was accessed and analysed through GEPIA2[42].

Zebrafish data acquisition and statistical analysis

All zebrafish larval engraftments were performed in biological duplicate, unless otherwise stated. All groups were >20 individuals per biological repeat, unless otherwise stated. All individuals were randomized and entered into either control or experimental groups, all individuals were randomly selected and imaged using the same exposure setting using a stereo fluorescent microscope. Outliers were removed from all data sets using GraphPad Prism 8.0, (Q5) prior to normalization and combination of all biological replicates. Data was normalized to either control (drug treatment) or to day one (in the case of growth kinetics experiments). Statistical significance was tested with an ANOVA, for normally distributed data sets, otherwise a Kruskal-Wallis test was used. Error bars depict ±SEM.

Patient data and statistical analysis

The statistical analyses were carried out with SPSS version 25 (IBM corp).

Correlation between melanin-related genes and chromosome 3 status and BAP1 status were calculated with Mann-Whitney U test. The survival analysis was carried out using Kaplan Meier survival curves and splitting the gene expression data in the middle and comparing the 32 patients with lower TYR, lower TYRP1 and lower DCT with the 32 patients with higher TYR, higher TYRP1 and higher DCT respectively. In the LUMC cohort, survival was calculated with melanoma-related mortality as the endpoint.

The TCGA cohorts for both UM and cutaneous melanoma were analyzed with the interactive web server GEPIA2, splitting the population along the median for each gene. In these cohorts, survival was calculated with overall survival as the endpoint.

Results

The presence of melanin and the upregulation of TYRP1 correlate with tumorigenic potential of UM PDX samples and with a decrease in disease-free survival in UM patients.

When studying the metastatic colonization capacity of uveal melanoma in a zebrafish model, we noticed striking differences between tumor samples. We had generated spheroid cultures from primary UM, as recently described by Groenewoud et al 2021. After dissociation of spheroids, cells were stained with a red transient dye and engrafted intravenously into blood vessels of reporter zebrafish larvae (*tg(fli:eGFP)*) at 48 hours post fertilization (hpf). We measured the engraftment over time based on the fluorescent intensity and the size of the metastatic foci, within the engrafted zebrafish larvae at 1-, 4-, and 6-days post injection (dpi) (Figure 1B). Of the three engrafted PDX samples, the highly-pigmented sample spUm-LB046 showed significant ($p<0.001$) enhancement of tumor cell number (as measured by fluorescence integrated density) over time, with many tumor cells visible all over the body after 6 days. Tumor sample spUm-LB048 (containing only medium levels of melanin) induced a significant enhancement of fluorescent signal between 1 dpi and 4 dpi ($p<0.001$), with almost total abrogation of the signal at 6 dpi ($p<0.001$), while the non-melanated primary UM sample spUM-LB049 was completely cleared from the engrafted zebrafish host at 4 dpi. We considered the option that the differences were caused by different degrees of melanin. As UM tend to spread hematogenously, we verified our findings by assessing the relation between tumor pigmentation and patient survival in a series of enucleated UM (LUMC cohort n=64) (Figure 1C). We used transcriptomics data to assess the effect of the transcription of the terminal enzymatic stages of melanin biosynthesis (Leiden cohort, Figure 1D). Pigmentation levels assessed after enucleation of primary UM sub-divided the tumors into two groups: non- and lightly-pigmented versus medium- and highly-pigmented tumors. Survival analysis indicated that there is a significant increase in melanoma-related death in patients with medium- and highly-pigmented tumors compared to those with non- and lightly-pigmented UM ($p=0.006$). When comparing melanin biosynthetic genes with melanoma-related death, only the final biosynthetic step of melanin synthesis demonstrated a correlation with bad disease outcome (*TYRP1*, $p=0.01$) whereas both upstream tyrosinase (*TYR*) and dopachrome tautomerase (*DCT*) were not related to

melanoma-related death (*TYR*, p=0.52; *DCT*, p=0.15). Overall, these results suggest that there is a causal link between the level of melanin in UM cells and their metastatic potential.

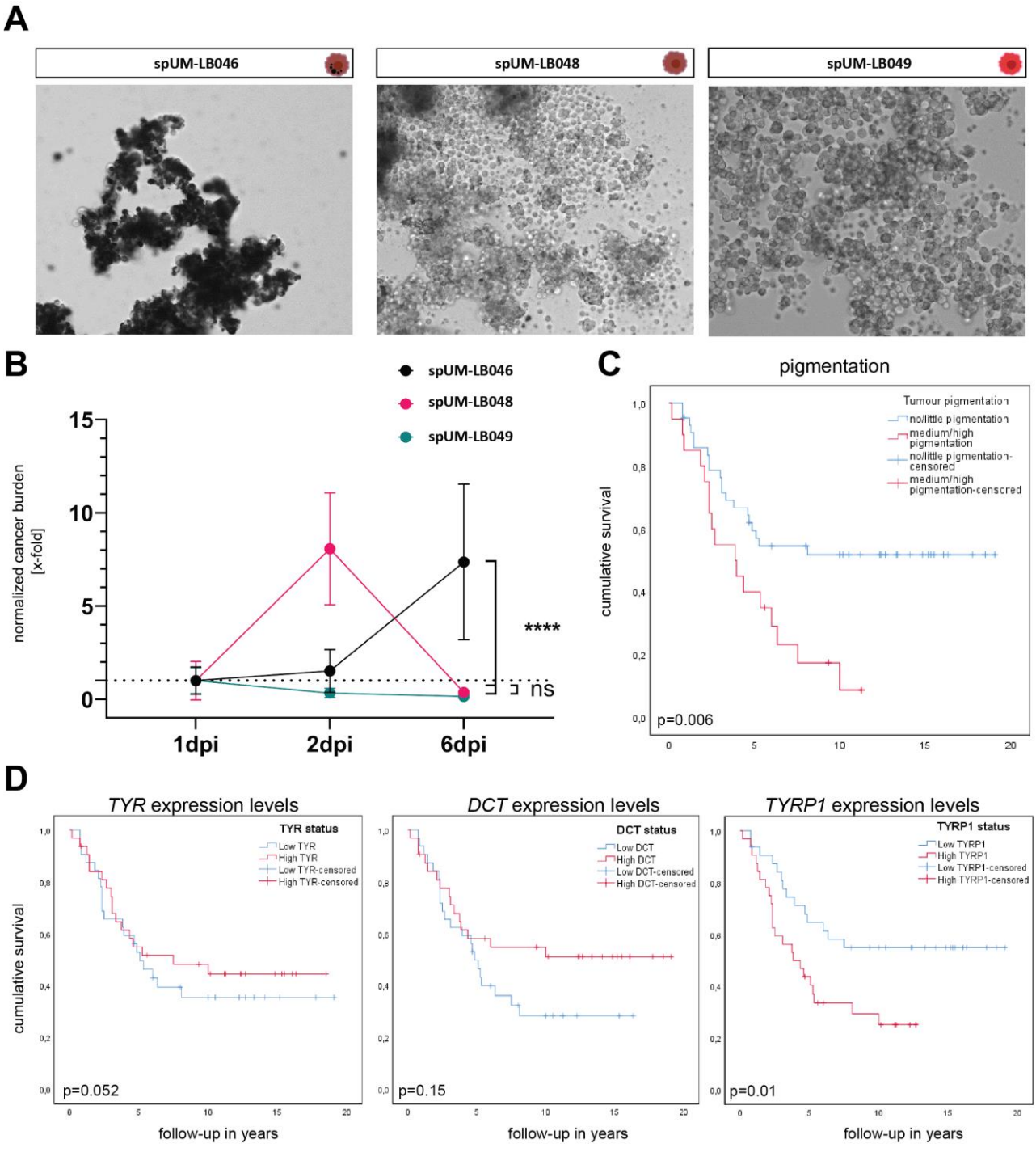

Figure 6 Melanin levels within primary UM cells correlate with survival *in vivo*. A) Three primary UM patient samples ranging from strongly melanated (spUm-LB046), intermediately melanated (spUm-LB048) and non-melanated (spUm-LB049). Melanin levels were derived from phase contrast images of spheroid cultures established from patient material, prior to engraftment. B) Three UM spheroid cultures were stained with red fluorescent lipid tracer (CMDiI) and then injected into zebrafish larvae and monitored for cancer cell engraftment on days 1, 4, and 6- post injection (dpi. C) Histological tumor pigmentation at the time of enucleation and their relation with survival of UM patients. Survival of patients with non and lightly-pigmented tumors (n= 43) was compared to survival in patients (n=20) medium- and highly-pigmented tumors based on pathological assessment. D) Assessment of the effect of individual melanin biosynthetic genes on UM survival. Expression of the most upstream located tyrosinase (TYR) and the downstream biosynthetic proteins dopachrome tautomerase (DCT, or alternatively TYRP2) and tyrosinase-related protein 1 (TYRP1), analyzed in a group of 64 patients; groups were determined according to the median mRNA expression only TYRP1 expression levels show a negative correlation with survival.

Chemical and genetic melanin depletion of highly-melanated CM melanoma cell line mugmel2 significantly reduces its metastatic potential.

After the primary assessment of the effect of melanin on metastatic dissemination of UM, we asked if this phenomenon could be extended to other melanomas. To determine this, we used a highly-melanated *RAS*-mutated CM cell line: mugmel2[31]. We first determined the presence of all stages of melanosome maturation in mugmel2 cells, using transmission electron microscopy (TEM) as shown in (Figure 2A). Melanosomes Type II, III and IV were readily visualized due to their intrinsic electron density, and are demarcated with yellow (▲ type II), blue (▲ type III) and red (▲ type IV) arrowheads, respectively. The eGFP-expressing mugmel2 cells were engrafted in zebrafish as described previously, with or without prior chemical depletion of melanin through 1-phenyl 2-thiourea (PTU). Intravenous injection of the melanin-depleted mugmel2 cells induced less metastatic colonization in *Casper* zebrafish at 6 dpi (Figure 2B) in comparison to non-depleted cells, and measured the effect of chemical melanin depletion on the total concentration of intracellular melanin *in vitro* (Figure 2D). We measured significant dose-dependent decreases of metastatic potential at 4 dpi and 6 dpi for two concentrations of PTU (125 and 500μM) when compared to treatment with equivalent volumes of vehicle control (DMSO) (Figure 2C). We showed a dose-dependent inhibition of intracellular melanin biosynthesis, when compared to vehicle control. The strongest inhibition, without deleterious effects on cell survival, was induced by 500 μM PTU (approximately 85%, $p<0.001$) and a dose-dependent

increase in melanin content between 500 μM and lower PTU concentrations ($p<0.05$) (Figure 2D). Concentrations of PTU >500 μM were deleterious to the proliferation and survival of the cells (results not shown).

Genetic interference with melanin biosynthesis through inhibition of tyrosine (*TYR)* expression by shRNA-mediated mRNA decay led to a significant inhibition of both melanin biosynthesis and intracellular melanin levels (Figure 2D)[20,32]. We used two individual shRNA constructs targeting *TYR.* This shRNA-mediated knock down of TYR in mugmel2 reduced the cells' metastatic capacity when compared to scrambled shRNA control concordantly (Figure 2E, $p<0.001$). To assess whether this decrease in metastatic capacity could be due to a decrease in overall migration, we measured cell migration *in vitro* using a wound healing assay. We observed no difference in the migratory potential when comparing PTU-treated cells with the vehicle control (Figure 2F, G). Using TEM, we determined whether PTU treatment induced loss of melanosomal structures in mugmel2 cells (Figure 2H). We observed a loss of type II, III and IV melanosomes upon treatment with both 500 and 250μM PTU (data for 250μM not shown). In summary, these data clearly suggest that the degree of melanation of mugmel2 correlates with its tumorigenic potential. The presence of all known stages of melanosomes indicates that cell line mugmel2 has retained its canonical melanogenic phenotype. The depletion of melanin from mugmel2 through either chemical or genetic means significantly alters its cellular tumorigenic capacity. This depletion does not significantly alter its migratory capacity suggesting that *in vitro* and *in vivo* functions of melanin inclusion are disjoined.

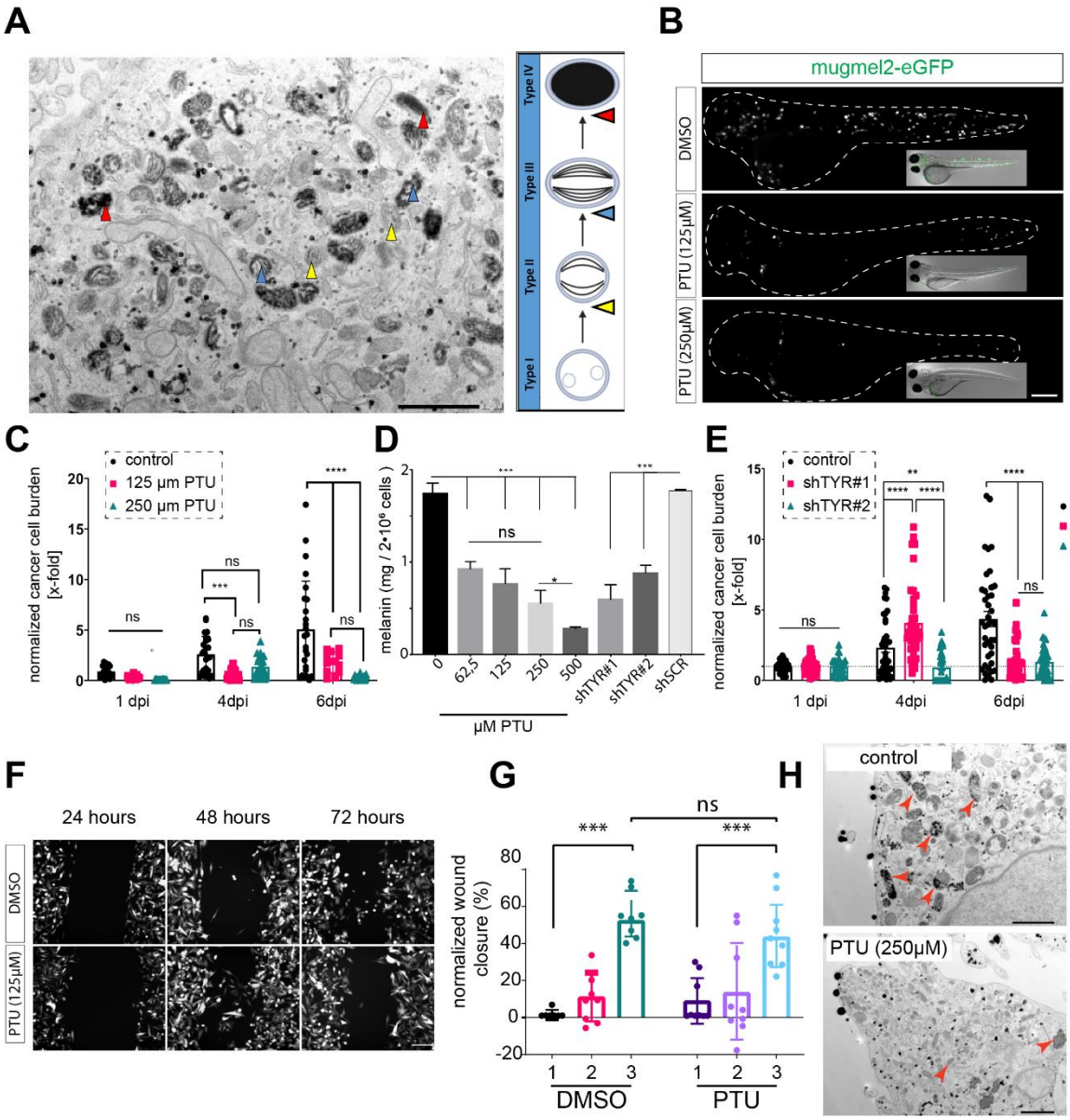

Figure 7 Melanin depletion of melanated melanoma cell lines decreases their tumorigenic potential. A) TEM assessment of melanosome maturation in mugmel2 cells: type II melanosomes are indicated by ▲, type III melanosomes by ▲ and type IV by ▲. Scale bars are 2 µm, and all images are representative images. B) Engraftment of melanotic melanoma cell line mugmel2 in non-pigmented CASPER zebrafish, confocal micrograph; cells were labeled with CMV:eGFP-blasticidin. Mugmel2 cells were treated with 1-phenyl 2-thiourea (PTU) *in vitro* prior to engraftment and its effect on cell intrinsic metastatic potential was compared to DMSO control C) PTU inhibition of mugmel2 melanation and its effect on the metastatic capacity of mugmel2 *in vivo*. Cells were depleted *in vitro* through PTU addition 2 weeks prior to hematogenous engraftment into CASPER zebrafish (n=2 * 20). Measurements were normalized to 1 day post injection (dpi), engraftment was monitored on 1, 4 and 6- dpi. D) Dose-dependent melanin depletion upon *in vitro* application of PTU to mugmel2 cells compared to solvent control and genetic depletion of TYR (lentiviral shRNA mediated knock down) compared to scrambled short hairpin control, as measured by spectrophotometer. E) Quantification of cancer cell engraftment

of zebrafish implanted with mugmel2-eGFP, containing shSCR, shTYR1#1 or shTYR1#2. Measurements were normalized to day 1 of each individual condition. F) Wound healing of mugmel2 cells treated with solvent control (DMSO) compared to PTU-mediated chemical depletion of melanin, shown as representative epifluorescent micrographs and in panel G) as quantification of wound area over time, normalized to wound area at t=0. H) TEM micrographs noting the chemical depletion of melanin and the subsequent reduction of visible melanosomes when compared to solvent control. The mean and the standard error of the mean were plotted (SEM), n=20*2. p<0.05=* p<0.01=** p<0.001=***.

Comparative analysis of pan-melanoma panel reveals a correlation between melanin levels, TYRP1 expression and tumorigenic capacity.

To further test our hypothesis that the presence of intracellular melanin plays a role in metastatic dissemination of different types of melanomas, we analyzed a matched panel of melanated and non-melanated melanoma cell lines (schematic representation in Figure 3A). The metastatic colonization in zebrafish was measured at 1, 4 and 6 dpi, comparing melanated and non-melanated cell lines derived from CoM (CRMM1, CRMM2), CM (SK-Mel28, PDX11917) and UM (XMM66 and OMM2.3). All tested cell lines were transduced with lentiviral tdTomato and data was analyzed after normalization of fluorescent intensity to 1 dpi (as described previously)[33]. For both CoM and CM, we noted a significantly enhanced metastatic colonization for the melanated cell line in the cell line pairs. Metastatic colonization did not seem exclusively linked to melanin content, CRMM1, p<0,001, as a melanated cell line and SK-Mel28, p<0,001 as a not visibly melanated cell line. PDX-derived CM cell line PDX11917 was found to be overtly melanated, both in culture and when pelleted during sub-cultivation, and showed only marginal proliferation in zebrafish, but was able to establish metastatic colonies at 6 dpi[34]. UM lines that were used in this panel were deemed to be non-metastatic and as expected failed to form any metastatic colonies, in a similar manner as reported by Groenewoud et al 2021. Subsequently, we determined if there were detectable melanosomes within the cell lines that made up our panel, to ensure that all our designated non-melanated cell lines indeed did not contain any melanosomes (Figure. 3D). Strikingly, not only CRMM1, PDX11917 but also SK-Mel28 showed active melanosome formation when observed using TEM. As an extension thereof and in line with the findings detailed in Figure 1, we asked if in this cell line panel, we could correlate *TYRP1* mRNA levels with their metastatic capacity (Figure 3E). We noted a significant increase of *TYRP1* expression in CRMM1,

PDX11917 and SK-Mel28 when compared to their non-melanated counter parts or when compared to the non-melanated cells within this panel ($p<0.001$). None of the non-melanated cell lines (CRMM2, XMM66, OMM2.3) showed detectable *TYRP1* mRNA.

Subsequently, we measured the effect of chemical inhibition of melanin biosynthesis on the metastatic colonization of highly-melanated PDX-derived CM cell line PDX11917 when compared to SkMel28, a cell line bearing only occult melanin. Here we demonstrated that PDX11917's metastatic capacity was significantly inhibited after chemical melanin depletion contrary to vehicle control, at 6 dpi ($p<0.01$). SkMel28 was not significantly inhibited by melanin depletion at 6 dpi, but instead displayed a significant delay in metastatic colonization at 4 dpi ($p<0.01$) when compared to DMSO control. SKMel28s tumorigenic capacity was eventually compensated by 6 dpi, and indicated no overall significant inhibition when compared to untreated control.

These observations suggest that the presence of melanin enhances a cell line's tumorigenic capacity and that TYRP1 levels are indicative of melanin biosynthesis, given that upstream activation is present. Strikingly, SkMel28 shows strong expression of TYRP1, but has only minimal melanosome formation and occult melanin, as visualized under TEM, under normal culture conditions. This further implies that the presence of melanin rather than solely the expression of TYRP1 is required for the enhancement of tumorigenic capacity.

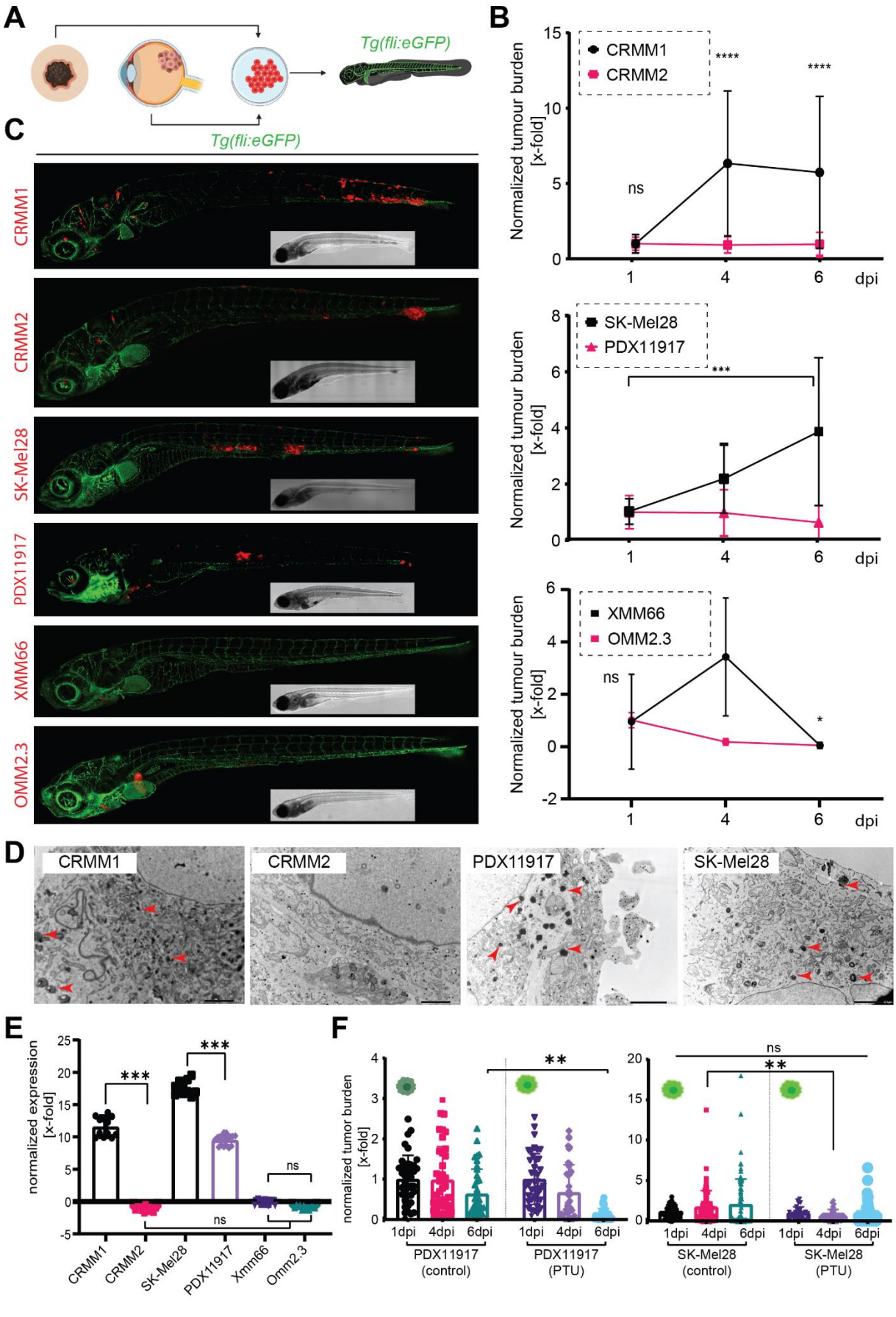
A
Tg(fli:eGFP)
Tg(fli:eGFP)
B
CRMM1
CRMM2
****
****
ns
Normalized tumour burden [x-fold]
dpi
SK-Mel28
PDX11917
***
XMM66
OMM2.3
ns
*
C
CRMM1
CRMM2
SK-Mel28
PDX11917
XMM66
OMM2.3
D
CRMM1
CRMM2
PDX11917
SK-Mel28
E
normalized expression [x-fold]
***
***
ns
ns
CRMM1
CRMM2
SK-Mel28
PDX11917
Xmm66
Omm2.3
F
normalized tumor burden [x-fold]
**
ns
**
1dpi 4dpi 6dpi
PDX11917 (control)
PDX11917 (PTU)
SK-Mel28 (control)
SK-Mel28 (PTU)

Figure 8 Engraftment of a (pan)melanoma panel in tg(fli:eGFP) zebrafish shows efficient engraftment of CM and CoM melanoma, whereas UM is readily cleared from zebrafish. A) Schematic representation of the experimental approach: CoM, CM and UM cell lines were injected in to Tg(fli:GFP) blood vessel reporter zebrafish through the duct of Cuvier at 48 hours post fertilization. Pairs of melanated and non- melanated cell lines were chosen for CoM and CM and two non-melanated cell lines for UM. B) Growth kinetics of the (pan)melanoma cell line panel, after hematogenous engraftment into zebrafish. For each experiment, 40 individuals were imaged, divided over two biological replicates. For all measurement, the integrated fluorescence density was plotted for 1, 4 and 6- dpi (all measurements were normalized to day 1 of the individual cell line). Measurements shown are the mean, error bars represent ± SEM. C) Confocal micrographs of representative phenotypes of the engrafted cell lines at 6 dpi D) Transmission electron micrographs of CoM and CM melanoma cell line pairs; (type IV melanosomes, indicated with ▲). Scale bars are 2 μm, all images are representative images. E) Quantitative PCR measurements of tyrosine related protein 1 (TYRP1), the enzyme responsible for the terminal biosynthetic conversion of tyrosine into melanin. F) Melanin depletion through PTU treatment of melanated and non-melanated cells. CM melanoma PDX-derived cell line PDX11917 and non-melanated melanoma cell line SK-Mel28 were depleted for 14 days prior to engraftment through injection into zebrafish. The mean and the standard error of the mean (SEM) were plotted, n=20*2. $p<0.05$=* $p<0.01$=** $p<0.001$=***.

Introduction of extraneous melanin re-instates UM metastatic potential.

We previously observed that UM cell lines are generally non-metastatic, non-melanated and do not express TYRP1. Many UM patients have a dark brown to black tumor at the time of enucleation, and we noticed that both a high level of pigmentation as well as a high TYRP1 expression correlate with poor survival (Figure 1C, D). Furthermore, the tested melanated primary samples (data for spUm-LB046 shown) were capable of establishing metastatic colonies in zebrafish (Figure1B).

To determine if introduction of extraneous melanin would be able to re-instate the metastatic potential of non-metastatic non-melanated UM cells, we established a co-culture system to allow *in vitro* transfer of melanin from donor melanated cells (mugmel2) to naïve UM cells (XMM66, OMM2.3) (Figure 4A, Supplementary Figure S1). We included a co-culture with vehicle (DMSO) in parallel to a melanin-depleted co-culture. Donor cells were pre-incubated with Mitomycin-C, a mitotic spindle poison, abrogating mitotic potential, while retaining overall cell viability; this allowed us to perform a protracted (72 hours) co-culture with the donor cells while blocking donor cell outgrowth. To determine how much melanin would be taken up, we measured the

intracellular melanin concentration in naïve UM cultures, UM cells co-cultured with melanated mugmel2 (mel+) and chemically melanin-depleted mugmel2 (mel-) cells. We noted a significant melanin enhancement in melanated co-cultures, for both UM cell lines compared to both naïve (2 to 3-fold) and melanin-depleted co-cultures (8 to 10-fold approximately) (Figure 4B). Using TEM, we verified the successful transfer of intracellular melanin from highly-melanated melanoma cell line mugmel2 (mugmel2 mel+) to XMM66 cells (Figure 4C). In naïve XMM66 cells, melanosomes were completely absent, whereas large melanosomal structures were observed in the co-cultures with melanated cells. In contrast, in the melanin-depleted co-culture, only a few small electron dense vesicles and some empty vesicles were observed (Figure 4C), indicating functional transfer of melanin from melanated CM donor cells to naïve non-melanated UM cells. Subsequently, we asked if the transferred intracellular melanin could play a protective role after UM cell injection into the bloodstream of zebrafish. We therefore injected these sets of co-cultured cells Xmm66 and OMM2.3 labeled with red fluorescent, co-cultured with green mugmel2mel+ and mugmel2mel- cells, into zebrafish and scored the metastatic burden at 6 dpi. In melanated co-cultures, both UM cell lines gained a significant enhancement in metastatic colonization in contrast to the melanin-depleted co-cultures (Figure 4D, E). Importantly these results proves that melanin inclusion into UM cells rescues their survival in circulation leading to metastatic dissemination.

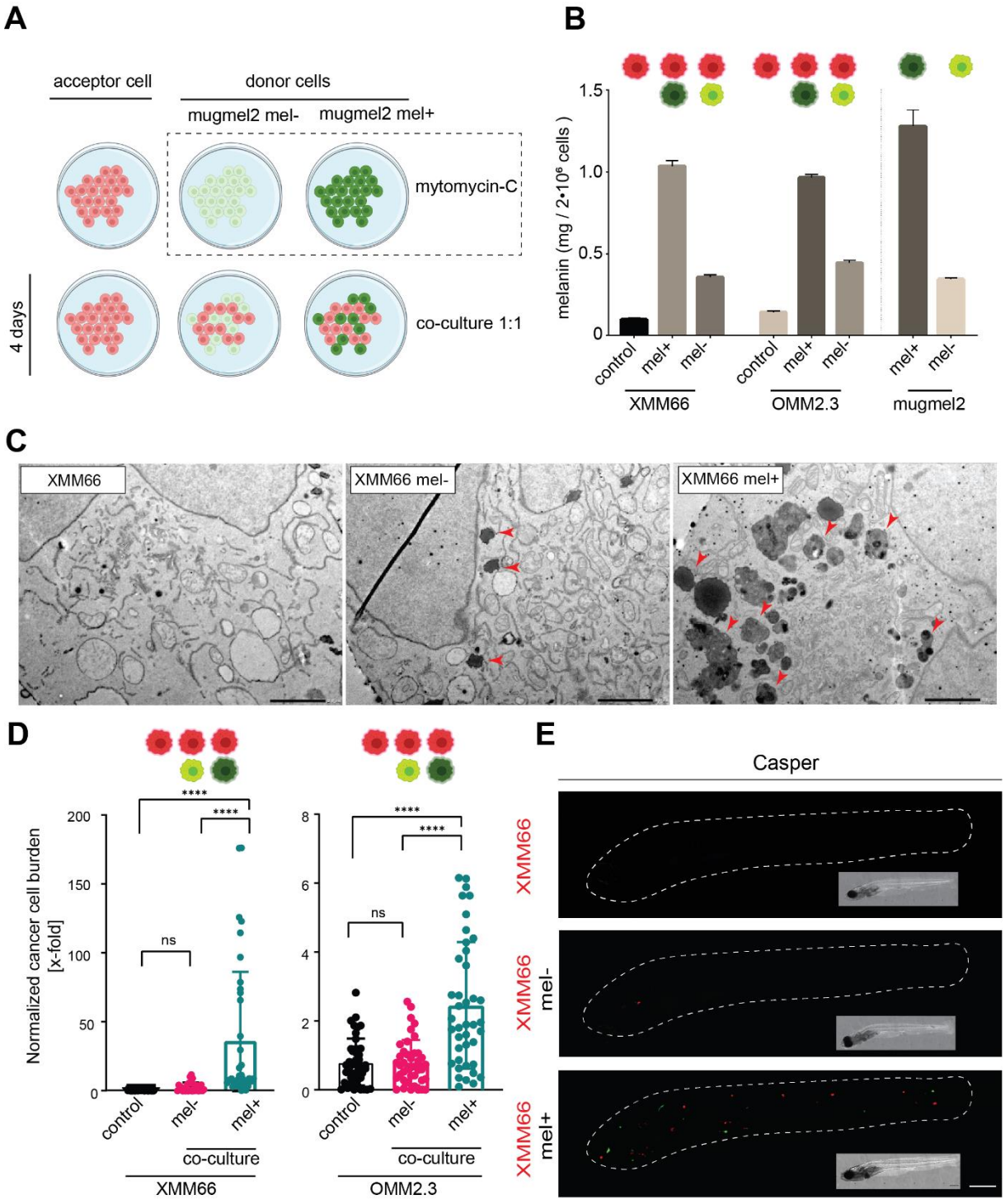

Figure 9 In vitro melanin transfer from donor (mugmel2) cells into recipient UM cells rescues their metastatic potential *in vivo*. A) Schematic representation of melanin transfer co-culture model. Recipient (red, UM cells) and donor cells (green, mugmel2, mugmel2 mel+, pre-treated with DMSO and mugmel2 mel- melanin depleted through pre-treatment with PTU) were cultured separately. Prior to co-culture, donor cells were pre-treated with mitomycin-C (100µg/mL) for 3 hours. Cells were mixed in a 1:1 ratio of acceptor cell combined with mel+ or mel- mugmel cells. After 4 days of co-culture, cells are harvested and either engrafted into zebrafish or used for *in vitro* analyses. B) Spectrophotometric analysis of uptaken melanin in UM cells, calculating mg / 2* 10^6 cells. Two individual experiments, 3

biological repeats. C) Representative transmission electron micrograph indicates the internalized melanosomes in UM cells donated from mugmel2 mel+ cells (type IV melanosomes, indicated with ▲). Scale bar represents 2 µm. D) End point measurement (6 dpi) of zebrafish (n=2 x 20) engrafted with naïve cells (control), UM cells co-cultured with melanin-depleted donor cells (mel-) and co-cultured with melanated donor cells (mel+). E) Representative fluorescent micrographs of co-cultured UM cell line XMM66, show the naïve XMM66 cells (red), XMM66 cells co-cultured with green melanin-depleted (mel-) and melanin-proficient (mel+) mugmel2 donor cells. Some mugmel2 cells (green) remain in circulation, do not form metastatic colonies but increase survival of UM cells as indicated in D.

Melanin protects against ferroptosis *in vivo*.

Successful metastatic colonization is a rare occurrence in most cancers and can be described by a stochastic process where random chance aligns with the metastatic cells intrinsic properties to allow a minute subset of cancer cells to form a metastatic colony in a suitable niche. Recent discoveries have highlighted the importance of reactive oxygen species (ROS) and more specifically ferroptosis in the curbing of metastatic dissemination in CM[7,35]. Since melanin has long been known to act as a ROS scavenger[18,19], we hypothesized that melanin might scavenge ROS while cells are in the circulation, thus prolonging circulating tumour cell (CTC) survival and thereby enhancing their chance of finding a suitable niche. The presence of melanin would thereby enhance a tumor's metastatic capacity. To address this hypothesis, we first tested the effect of melanin depletion on ROS induction *in vitro,* measured by CellRox fluorescent assay. CellRox utilizes a dye that becomes highly fluorescent after ROS-mediated oxidation. We measured a significant enhancement in the level of induced ROS in melanin-depleted mugmel2 cells visualized by CellRox: melanin depletion by pre-treatment with PTU led to increased ROS production following a challenge with ROS inducers Menadione, Paraquat and H_2O_2 (Figure 5A, B)., Moreover, the imaging clearly shows that at the time of analysis most of the melanin-depleted cells have been killed by the ROS inducers while the melanated control (DMSO pre-treated) cells were still adherent to the culture plate. These results suggest that melanin-depleted cells are more sensitive to ROS induction.

Due to the recent publications linking ferroptosis to the curbing of metastatic dissemination[7], we reasoned that ferroptosis might be the leading cause of ROS-mediated cell death. These findings are supported by our previous observation, where melanin retained in cells protects them during metastatic dissemination. To assess the

specific growth inhibitory effect of known ferroptosis-inducers erastin and RSL3, we performed a WST1-based proliferation assay on both melanin proficient and deficient mugmel2 cells (Figure 5C). Strikingly, we noted that mugmel2 (derived from an NRAS-driven cutaneous melanoma) was, in normal culture conditions, refractory to the entire concentration range of either erastin or RSL3 (2-fold dilution series, 10 to 0,039 µM, data not shown). To more accurately mimic the biological situation *in vivo,* we subsequently repeated the experiment with lowered glutamine and fetal bovine serum concentrations. We found that in these *in vitro* conditions, only melanin-depleted mugmel2 was significantly sensitized to both erastin (approximate growth inhibition 70-80%, 10-0.625 µM, $p<0.001$) and RSL3 (approximate growth inhibition 60-80%, 10-1,25 µM, $p<0.001$ and 0.625 at $p<0.05$). In contrast, the melanin-proficient mugmel2 remained refractory to erastin and were only susceptible to the highest concentrations of RSL3 (10 and 5 µM, $p<0.001$). Finally, we determined if the growth inhibitory effect of ferroptosis would translate to an *in vivo* situation. To this end, we injected intravenously zebrafish larvae with our previously described set of melanoma cells (UM, CM and CoM), at 48 hpf and treated the engrafted larvae from 1 dpi with 5 µM erastin and 10 µM RSL (Figure 5D). We subsequently measured the tumor burden at 6 dpi and normalized the tumor burden to the vehicle control (DMSO). We noted that CoM cell lines CRMM1 and CRMM2 and CM cell line SK-Mel28 showed a significant ($p<0.001$) reduction of tumor burden when treated with erastin. Mugmel2 was insensitive to this treatment. RSL3 did not reduce tumor burden in any of the tested cell lines, although it did induce a clear, yet non-significant reduction in tumor burden using cell lines CRMM1 and SK-Mel28. Subsequently, we assessed the efficacy of ferroptosis induction in mugmel2 after melanin depletion, *in vivo*, through both genetic and chemical means, reasoning that through melanin depletion we could sensitize this refractory cell line to ferroptosis-mediated cell death. We engrafted zebrafish larvae as previously described (Figure 5D) with mugmel2 depleted from melanin through chemical and genetic means and treated the engrafted larvae from 1 dpi with 5 µM erastin and 10 µM RSL (Figure 5E). We determined the tumor burden, normalized to vehicle control (DMSO) at 6 dpi. There is no significant sensitization to erastin, most likely due to its strong inhibitor capacity on the melanated sample as well. Strikingly RSL3, acting through GPX4, strongly reduced the tumor burden in chemically as well as genetically-melanin depleted populations, indicative of resistance to canonical ferroptosis mediated by melanin.

In conclusion, these data suggest that melanin protects melanoma cells in circulation, functionally mitigating intracellular ROS and protecting circulating cancer cells from ferroptotic cell death, indirectly enhancing tumorigenic capacity.

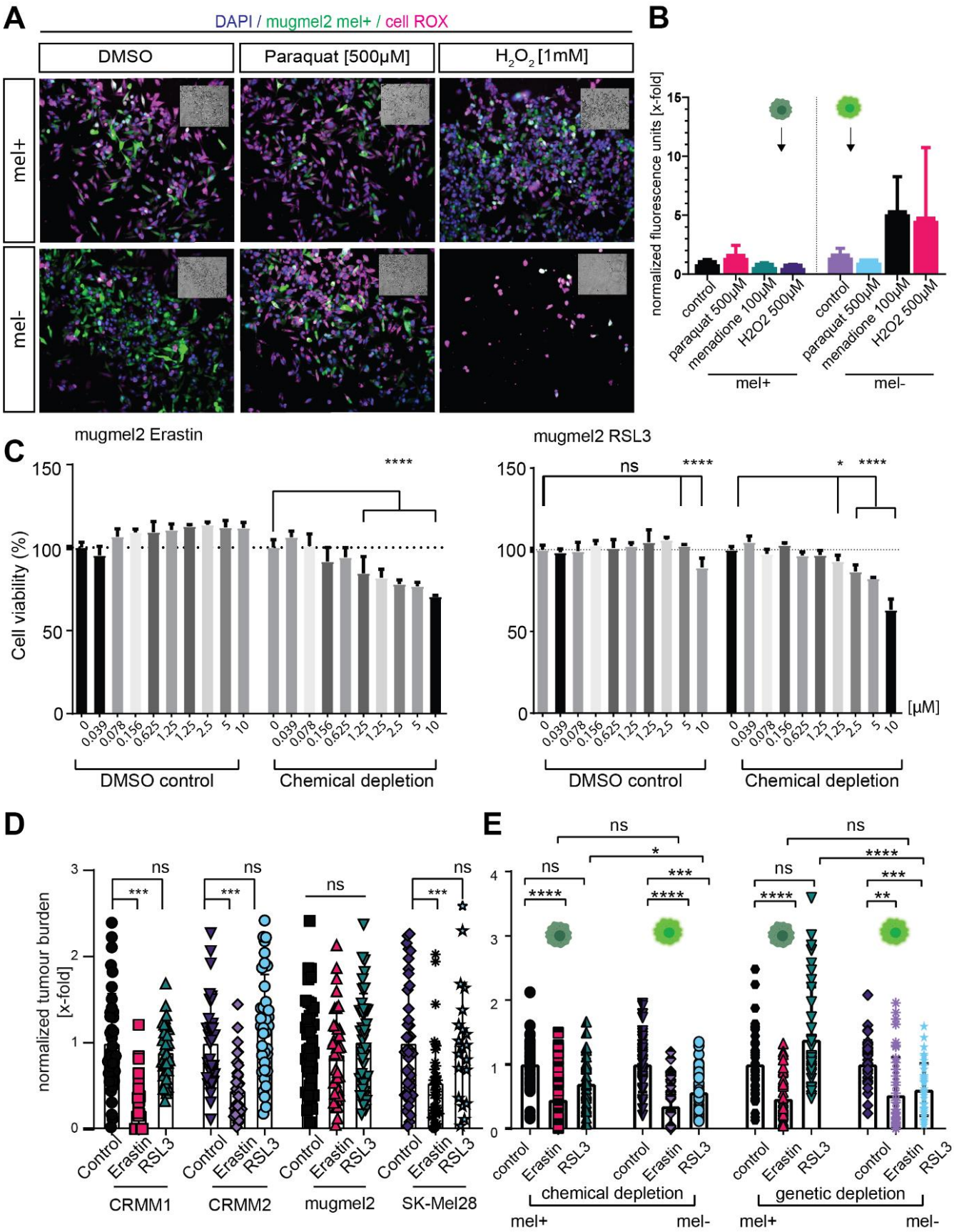
A
DAPI / mugmel2 mel+ / cell ROX
DMSO
Paraquat [500µM]
H2O2 [1mM]
mel+
mel-
B
normalized fluorescence units [x-fold]
control
paraquat 500µM
menadione 100µM
H2O2 500µM
mel+
mel-
C
mugmel2 Erastin
mugmel2 RSL3
Cell viability (%)
[µM]
DMSO control
Chemical depletion
D
normalized tumour burden [x-fold]
Control
Erastin
RSL3
CRMM1
CRMM2
mugmel2
SK-Mel28
E
chemical depletion
genetic depletion
mel+
mel-

Figure 10 ROS and ferroptosis is quenched by intracellular melanin, erastin induces ferroptosis at sufficient levels to overcome cellular ROS defenses. A) CellRox fluorescent ROS measurement of mugmel2 cells with (mel-) and without melanin (mel+) depletion through PTU pre-treatment, as described previously (i.e. in Figure 2D). All wells were seeded with $5{,}0*10^4$ cells per well and treated with ROS inducers for 60 min and imaged after fixation. Paraquat, menadione and H_2O_2 were used to induce non-specific intracellular ROS. Nuclei are stained with 4,6-diamidino-2-phenylindole (DAPI), cells are stained with cytoplasmic GFP (shown as green), CellRox deep red (shown as magenta). B) Quantification of CellRox signal, through epifluorescent imaging and subsequent processing. All measurements were normalized for the number of remaining cells using the number of nuclei ($DAPI^+$) and only CellRox signal within the GFP-positive cells were measured; measurements were repeated twice with 3 biological repeats. C) Represents *in vitro* proliferation (WST1) assay to assess the growth inhibitory effects of ferroptosis inducers erastin and RSL3 on mel+ and mel- mugmel2 cells. D) Ferroptosis induction in ZF xenograft models *in vivo* obtained by engraftment of a melanoma panel with CoM (CRMM1 and CRMM2) and CM cell lines (SK-Mel28 and mugmel2). Ferroptosis inducers erastin and RSL3 were added to the previously determined maximum tolerated dose (MTD) (results not shown, manuscript in writing, erastin 5 µM and RSL3, 10 µM) to the eggwater of engrafted larvae at 3 dpi. The water containing the compounds was exchanged every other day. At 6 dpi, the cancer cell burden was measured and subsequently normalized to the vehicle control group (of each individual condition). E) *In vivo* ferroptosis induction as described in D in larvae engrafted with naïve mel+ and depleted (mel-) mugmel2 cells after chemical (PTU) and genetical (shTYR#2) melanin depletion prior-engraftment. Melanin depletion by chemical and genetics means sensitized melanoma cell lines to RSL3 whereas erastin mainly seems to circumvent or overpower ferroptosis resistance mediated by melanin.

Translational value and future implementation of pro-ferroptotic strategies for the treatment of melanomas.

These findings led us to search for both elevations in GPX4 levels or alterations in melanin biosynthesis in CM and UM patient survival data (Figure 6). We compared TCGA datasets, analyzing the effect of melanin biosynthetic genes on overall survival (Figure 6A). We subsequently focused on the effect of melanin biosynthetic genes on overall survival of CM patients in a group of 458 patients and were able to demonstrate a strong effect of melanin biosynthetic molecules. All melanin biosynthetic pathway genes assessed in this manner correlated negatively with patient overall survival (Figure 6 B, *MITF*, p=0.022; *TYR*, p=0.03; *DCT*, p=0.038; *TYRP1* p=0.0019).

For UM, using the Leiden data set, a high expression level of GPX4 strongly correlated with a reduction in overall survival, whereas melanin biosynthetic activity as assessed by mRNA levels of TYRP1 revealed an even stronger negative relation with survival of primary UM patients (Figure 1D). Mitochondrial voltage-gated anion channel

(VDAC) is another target for the induction of ferroptosis, and one of the erastin targets. We assessed the relation between VDAC levels and survival of CM and UM patients and showed that high VDAC1 expression was significantly correlated with a reduced overall survival time for both melanomas (Figure 6C). No transcriptomics data was available to us for CoM melanoma at the time of writing. Taking together the experimental data linking melanin to ferroptosis resistance, ferroptosis susceptibility and the transcriptional data presented in this manuscript, we generated a model (Figure 6D). We propose that in the cancer cell, melanin forms a physical depot with ROS-absorptive properties. This functions to protect cancer cells in the circulation from ROS and more specifically, ferroptosis. Cells are thus protected from slow increases in ferroptotic stimuli, as indicated through the intrinsic resistance of strongly-melanated cells to GPX4 inhibition (RSL3) mediated-ferroptotic cell death. Sharp increases in ferroptotic ROS through inhibition of VDAC function through treatment with erastin overwhelm the anti-ferroptotic function of melanin.

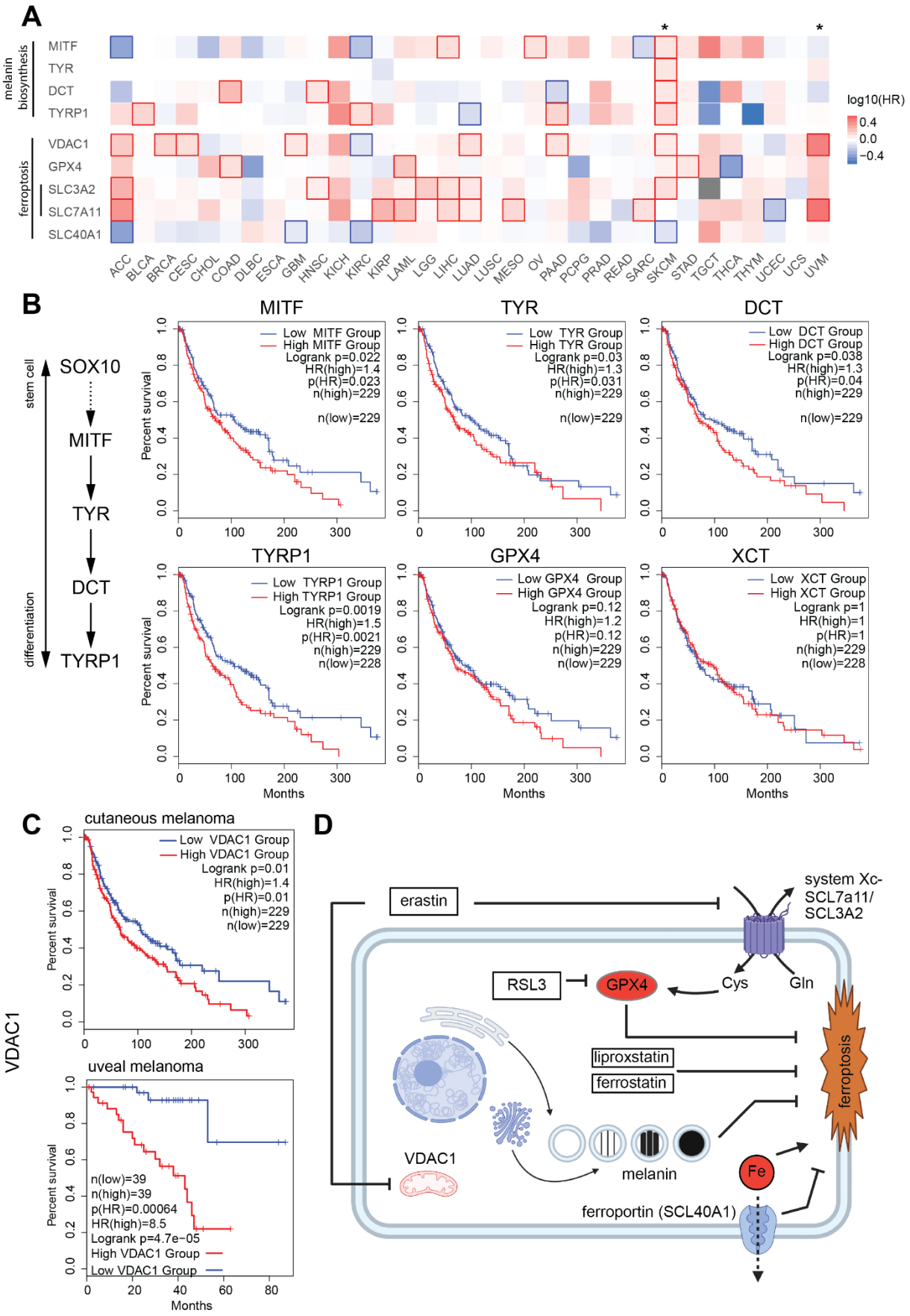
A
melanin biosynthesis
MITF
TYR
DCT
TYRP1
ferroptosis
VDAC1
GPX4
SLC3A2
SLC7A11
SLC40A1
log10(HR)
0.4
0.0
−0.4
ACC BLCA BRCA CESC CHOL COAD DLBC ESCA GBM HNSC KICH KIRC KIRP LAML LGG LIHC LUAD LUSC MESO OV PAAD PCPG PRAD READ SARC SKCM STAD TGCT THCA THYM UCEC UCS UVM
B
stem cell
SOX10
MITF
TYR
DCT
TYRP1
differentiation
MITF
Low MITF Group
High MITF Group
Logrank p=0.022
HR(high)=1.4
p(HR)=0.023
n(high)=229
n(low)=229
TYR
Low TYR Group
High TYR Group
Logrank p=0.03
HR(high)=1.3
p(HR)=0.031
n(high)=229
n(low)=229
DCT
Low DCT Group
High DCT Group
Logrank p=0.038
HR(high)=1.3
p(HR)=0.04
n(high)=229
n(low)=229
TYRP1
Low TYRP1 Group
High TYRP1 Group
Logrank p=0.0019
HR(high)=1.5
p(HR)=0.0021
n(high)=229
n(low)=228
GPX4
Low GPX4 Group
High GPX4 Group
Logrank p=0.12
HR(high)=1.2
p(HR)=0.12
n(high)=229
n(low)=229
XCT
Low XCT Group
High XCT Group
Logrank p=1
HR(high)=1
p(HR)=1
n(high)=229
n(low)=228
Percent survival
Months
C
VDAC1
cutaneous melanoma
Low VDAC1 Group
High VDAC1 Group
Logrank p=0.01
HR(high)=1.4
p(HR)=0.01
n(high)=229
n(low)=229
uveal melanoma
n(low)=39
n(high)=39
p(HR)=0.00064
HR(high)=8.5
Logrank p=4.7e−05
High VDAC1 Group
Low VDAC1 Group
Percent survival
Months
D
erastin
system Xc-
SCL7a11/
SCL3A2
RSL3
GPX4
Cys
Gln
liproxstatin
ferrostatin
ferroptosis
VDAC1
melanin
Fe
ferroportin (SCL40A1)

Figure 6 **Analysis of transcriptional activity of melanin biosynthesis in CM melanoma patient material (TCGA, accessed through GEPIA).** A) Survival map of all available TCGA cancer data sets, comparing the effect of melanin biosynthesis genes on melanoma-related survival (CM melanoma (SKCM) and UM (UVM) are noted with an asterisk, additional abbreviations can be found in supplementary figure S3), significant effect on survival is denoted with a red bounding box. In CM melanoma (n= 458), a significant negative correlation with disease free survival for all known melanin biosynthetic genes can be noted (MITF, TYR, DCT, TYRP1) whereas in UM (n=78), only TYR and TYRP1 show no significant correlation to overall survival. Similar comparative analysis of the TCGA, plotting the correlation of disease-free survival for the known anti-ferroptotic mechanisms, system Xc- (SCL7A11 and SCL3A2), ferroportin (SCL40A1), GPX4 and mitochondrial VDAC1 show that there is a significant effect of SCL3A2 on survival in CM (p=0.00022, data not shown) and SCL7A11 in UM (p=0.00014, data not shown). Moreover, both CM and UM display a significant reduction in overall survival for patients with a high expression of VDAC1. B) comparative analysis of the effect of melanin biosynthetic gene expression on disease free survival in CM melanoma patients (TCGA data). All known major melanin biosynthetic genes negatively correlate with overall survival (MITF, p=0.022; TYR, p=0.03; DCT, p=0.038; TYRP1 p=0.0019). Analysis of ferroptosis detoxifying enzymes GPX4 and XCT (synonymous with SCL7A11) shows that only GPX4 correlates negatively with overall survival. Expression of SOX10 did not yield any correlation with disease free survival (p=0.19, data not shown). TCGA SKCM cohort size = 458, all values are split along the median for each gene. C) erastin (one of the main and most potent inducers of ferroptosis) is thought to act through the perturbation of VDAC function, releasing reactive oxygen into the cytoplasm from mitochondria. Analysis of the effect of VDAC1 on CM and UM disease free survival, indicate that VDAC1 expression significantly influences survival (CM, p=0.01; UM, p=0.00064). D) model of the proposed mechanisms of melanin-mediated ROS resistance in melanoma cells.

Discussion

Melanomas are often strongly pigmented in patients. The prevalence of melanoma pigmentation underlines not only the cellular lineage they derive from, but also the presence of selection pressure forcing the expression of melanin-related genes. Cells derived from pigmented melanomas generally lose their melanin biosynthetic capacity and increase their migratory capacity *in vitro*[22]. Next to clinical correlations that associate either melanin or melanin-related gene signatures with a bad disease outcome, the true functional role of melanin in melanoma development remains unclear and contradictory[21,36].

We engrafted spheroids derived from primary UMs tissues in zebrafish and observed that there was a relation between the presence of melanin in the primary UM samples (clinically scored for melanotic level in a +, +/- and – scale) and prolonged circulation and tumorigenic potential in zebrafish after engraftment. This experiment indicated that there is a significant difference in tumorigenic potential of heavily-melanated patient samples when compared to both intermediate and lightly-melanated samples. Interestingly, UM cell lines OMM2.3 and XMM66, originally derived from metastatic UM, had lost all melanogenic capacity *in vitro*, and were readily cleared from the engrafted host after systemic injection (within 16 hours post injection). This observation and the short timeframe, wherein near complete attrition of CTCs is attained, is in line with a possible induction of ROS-mediated cell death[8]. Strikingly, we observed strong tumorigenic capacity when engrafting low passage spXMM66 cells, derived from a pigmented patient-derived xenograft tissue (PDX), while an immortalized cell line from the same patient XMM66 proved to be non-tumorigenic. In addition, our analysis of a clinical UM cohort confirmed a strong association between high tumor pigmentation, high expression of *TYRP1*, the terminal melanin biosynthetic, and high UM-related death in patients (LUMC cohort n=64).

Following this observation, we reasoned that this phenomenon might hold true for other melanoma sub-types. We concordantly observed that there has been a nearly complete loss of melanin biosynthesis in most melanoma cell lines, presumably through negative selection (or general lack of selection pressure) by successive *in vitro* cultures without selection pressure.

To assess this, we acquired the aberrant CM cell line mugmel2, an NRAS-driven and heavily-melanated melanoma cell line[31]. We assessed the formation of melanosomes using TEM and measured melanin levels using a spectrophotometric method described by Friedmann et al[18]. Both chemical and genetic inhibition of melanin biosynthesis, by treatment with 1-Phenyl-2-thiourea (PTU) or *TYR1* shRNA interference, reduced melanin levels and decreased metastatic dissemination in zebrafish xenografts.

We assembled a set of UM, CM and CoM melanoma cell lines and were able to generate a set of paired melanated and non-melanated CM and CoM cell lines. We repeated the chemical depletion of melanin in the CoM melanoma set and found that also within this set there is a significant reduction of tumorigenic potential upon depletion of melanin, suggesting that melanin has a canonical pro-tumorigenic function in all melanomas. Strikingly, our findings validate the work from Pinner et al 2009, where they state that low melanation correlates with high migratory capacity of CM cells *in vivo*, but that melanated cells do generate more distant metastases[22].

To assess the mechanistic effect of melanin levels on the metastatic behavior of UM cell lines we developed a co-culture system to transfer melanin from mugmel2 donor cells into UM acceptor cells. Through this system, we introduced exogenous melanin to UM cells, for subsequent assessment of metastatic capacity. Other methods to re-instate melanin biosynthesis were unsuccessful (treatment with a-MSH, forskolin or lentiviral over-expression of melanin biosynthetic genes *DCT*, *TYR* and *TYRP1*, results not shown). Spectrophotometric measurement of the uptake of melanin and visualization of melanosomes through TEM confirmed that UM cells readily take up melanin from external donors. Co-cultures of both melanin biosynthesis proficient and deficient donor cells were generated and we measured a significant enhancement of detected melanin in co-culture with melanin proficient donors when compared to melanin deficient donors or untreated control cells. Both OMM2.3 and XMM66 co-cultured with melanin-proficient cells showed a significant enhancement in tumorigenic potential when compared to either co-culture with melanin deficient or untreated cells. These findings indicate that UM cells are capable of up taking melanosomal melanin, at least *in vitro,* and underscore one of the possible functions of melanin in the distant metastasis of UM.

Taking together our observations with recently published experimental proof that circulating melanoma cells are largely killed through reactive oxygen[7,35], we hypothesized that ROS-based cell death might be the underlying mechanism driving UM attrition in circulation[7]. In line with this hypothesis, melanin inclusion within UM cells might thus help prevent *in vivo* cell death of circulating UM cells. More recently there has been experimental proof that circulating tumor cells are killed specifically by an iron-dependent non-apoptotic cell death mechanism known as ferroptosis[35].

Using our model, we tested if melanoma cells were responsive to the induction of ferroptosis during their time in circulation in the zebrafish model. We started out by challenging duplicate sets of melanated and non-melanated melanoma cells we used previously and demonstrated a clear correlation between the levels of melanation and the response to the induction of ferroptosis with inhibitors of GPX4 ((1S,3R)-RSL3; alternatively named RSL3) and system Xc- (erastin)[23,25,27,37]. Ferroptosis induction by erastin occurs through perturbation of system Xc- and mitochondrial voltage-dependent anion channels[26,37]. The *in vivo* induction of ferroptosis with erastin proved to be highly effective, reducing tumor burden independent of melanin inclusion for cell line SK-Mel28, which showed low level melanation under TEM. Additionally, erastin proved sufficiently potent to induce ferroptosis in strongly-melanated mugmel2 cells. Although there was a trend indicative of sensitization of SK-Mel28 cells to erastin by melanin depletion, this was presumably negated by the strong effects of erastin on the mel+ population.

Furthermore, we showed that there was a melanin-dependent sensitivity to ferroptosis induction, when melanin-depleted mugmel2 cells were compared with melanated mugmel2 cells. Ferroptosis was induced either directly through the inhibition of GPX4 or indirectly by blocking the glutamate antiporter function of the system Xc- (erastin) and concordant perturbation of VDAC function. We found that mugmel2, derived from an NRAS-driven CM, is largely refractory to ferroptosis induction *in vitro* under conventional conditions, whereas these cells can be sensitized through depletion of glutamine (a co-factor for GPX4 function). The ferroptosis refractory nature of this RAS-driven cell line is contra-dogmatic, as both RSL3 (RAS specific lethal 3) and erastin have been selected through a RAS hyperactivation specific *in vitro* synthetic lethal screen[37]. Therefore, we reason that chemical depletion of melanin sensitizes mugmel2 cells to ferroptosis. This highlights the functional relationship between the

presence of melanin and ferroptosis resistance, *in vitro*. Only ferroptosis induction through GPX4 inhibition induced a significant difference between melanated and non-melanated mugmel2 cells, indicating that non-melanated cells are more susceptible to canonical ferroptosis induction through inhibition of GPX4.

These findings led us to search for both elevations in GPX4 levels or alterations in melanin-biosynthesis genes (*MITF, TYR, DCT, TYRP1*) in patient survival data, where we found that a high expression of GPX4 in CM significantly correlated with decreased overall survival. A high tumor expression of all melanin biosynthetic genes was correlated with increased death in CM patients. Strikingly, there were only insignificant reductions when correlating ferroptosis mediators *GPX4* and *SCL7A11* to overall survival of CM patients, on a whole tumor level. This however does not exclude the presence of inter-tumoral differences.

For UM we found that a higher GPX4 expression strongly correlated with shorter survival, whereas melanin biosynthetic activity when assessed as a measure of mRNA levels of TYRP1 showed an even stronger negative relation with survival of primary UM patients. No transcriptomics data was available to us for CoM melanoma at the time of writing.

VDAC1, one of the putative targets of erastin, showed a significant negative correlation relation with patient survival for both CM and UM. This finding is in line with the strong inhibitory effect of erastin and explains erastin's strong inhibitory capacity on circulating cancer cells irrespective of intracellular melanin levels. Our findings are in line with Nawarak et al 2008, who show that arbutin, a known skin whitening agent and inhibitor of TYR, works by enhancing VDAC1 protein levels in A375 melanoma cells[38].

Taken together, our findings establish a functional link between intracellular melanin levels in melanoma cells irrespective of their tissue of origin. Cells containing melanin survive longer in the circulation of zebrafish during experimental micro-metastasis formation and hence display an enhanced capacity to establish micro-metastatic colonies. In line with the elegant experiments performed by Pinner et al in 2017[22], melanin content lowers (albeit in our hands not significantly so) the migration capacity of melanated cells (endogenously or exogenously melanated). Here our findings prove

that metastatic dissemination and metastatic initiation is effectively enhanced by the presence of intracellular melanin.

The biological function of melanin as a ROS quencher is widely accepted[13,14,19]. Furthermore, there are several studies that correlate melanin concentrations, either through direct measurements of melanin levels or through the detection of blood borne mRNA in CM patients, with a worse prognosis[21,36]. Paradoxically, there are experimental studies showing a converse role of melanin, inhibiting small scale metastasis in animal models[21,22]. Taken together, we reason that our findings bridge the gap between the observed phenomenon in patients and the discrepancy in experimental animal models by showing that melanated melanoma cells have a survival advantage *in vivo* in the blood circulation and are more resistant to ferroptosis. Furthermore, we show, using available patient survival data (TCGA and LUMC cohort for UM), that CM, UM patients have a worse prognosis when melanin biosynthesis is upregulated, notably the expression of terminal melanin biosynthetic enzyme TYRP1. VDAC1 was identified as another gene associated with a negative disease outcome and is a potential target for future therapy.

Acknowledgements:

We kindly thank Emilie Vinolo for the managerial assistance provided during this UMcure2020 project.

This work has received funding from the European Union's Horizon 2020 research and innovation program under grant agreement No 667787 (UM Cure 2020 project, www.umcure2020.org).

We kindly thank Prof. R. Hoeben and M. Rabelink (Department of Cell Biology, LUMC) for providing shRNA (lentiviral) vectors (TRC library, Sigma-Aldrich)

All graphics (excluding scientific data) were generated using Biorender.com

The results shown here are in whole or part based upon data generated by the TCGA Research Network: https://www.cancer.gov/tcga accessed through gepia(2)

AG Conceived, performed, analyzed all experiments and interpreted all the data (unless otherwise stated), wrote the manuscript.

MCG performed the UM patient pigment data analysis, and provided feedback on the manuscript.

JY performed *in vitro* proliferation assays, read the manuscript.

GEML performed all the TEM sample prep and data acquisition, read the manuscript.

MJJ supplied materials and reviewed the manuscript.

BES-J provided funding, supervised the project and reviewed the manuscript.

References

1. Mehlen, P. & Puisieux, A. Metastasis: A question of life or death. *Nature Reviews Cancer* vol. 6 449–458 (2006).

2. Bayraktar, S. & Glück, S. Molecularly targeted therapies for metastatic triple-negative breast cancer. *Breast Cancer Res. Treat.* **138**, 21–35 (2013).

3. Balch, C. M. *et al.* Final version of 2009 AJCC melanoma staging and classification. *J. Clin. Oncol.* **27**, 6199–6206 (2009).

4. Chiang, A. C. & Massagué, J. Molecular Basis of Metastasis. *N. Engl. J. Med.* **359**, 2814–2823 (2008).

5. Weiss, L. Metastatic Inefficiency. *Adv. Cancer Res.* **54**, 159–211 (1990).

6. Luzzi, K. J. *et al.* Multistep Nature of Metastatic Inefficiency : Dormancy of Solitary Cells after Successful Extravasation and Limited Survival of Early Micrometastases. *Am. J. Pathol.* **153**, 865 (1998).

7. Piskounova, E. *et al.* Oxidative stress inhibits distant metastasis by human melanoma cells. *Nature* **527**, 186–191 (2015).

8. Chandra, J., Samali, A. & Orrenius, S. Triggering and modulation of apoptosis by oxidative stress. *Free Radic. Biol. Med.* **29**, 323–333 (2000).

9. NC, J. & D, G. Role of melanin in melanocyte dysregulation of reactive oxygen species. *Biomed Res. Int.* **2013**, (2013).

10. Yang, H. *et al.* The role of cellular reactive oxygen species in cancer chemotherapy. *J. Exp. Clin. Cancer Res. 2018 371* **37**, 1–10 (2018).

11. Kumari, S., Badana, A. K., G, M. M., G, S. & Malla, R. Reactive Oxygen Species: A Key Constituent in Cancer Survival. *Biomark. Insights* **13**, (2018).

12. Liou, G.-Y. & Storz, P. Reactive oxygen species in cancer. *Free Radic. Res.* **44**, 479–496 (2010).

13. Brenner, M. & Hearing, V. J. The Protective Role of Melanin Against UV Damage in Human Skin. *Photochem. Photobiol.* **84**, 539 (2008).

14. GJ, F. *et al.* Mechanisms of photoaging and chronological skin aging. *Arch. Dermatol.* **138**, 1462–1470 (2002).

15. Noonan, F. P. *et al.* Melanoma induction by ultraviolet A but not ultraviolet B radiation requires melanin pigment. *Nat. Commun. 2012 31* **3**, 1–10 (2012).

16. Cichorek, M., Wachulska, M., Stasiewicz, A. & Tymińska, A. Skin melanocytes: biology and development. *Adv. Dermatology Allergol. Dermatologii I Alergol.* **30**, 30 (2013).

17. Li, M., Knapp, S. K. & Iden, S. Mechanisms of melanocyte polarity and differentiation: What can we learn from other neuroectoderm-derived lineages? *Curr. Opin. Cell Biol.* **67**, 99–108 (2020).

18. Friedmann, P. S. & Gilchrest, B. A. Ultraviolet radiation directly induces pigment production by cultured human melanocytes. *J. Cell. Physiol.* **133**, 88–94 (1987).

19. Denat, L., Kadekaro, A. L., Marrot, L., Leachman, S. A. & Abdel-Malek, Z. A. Melanocytes as instigators and victims of oxidative stress. *Journal of Investigative Dermatology* vol. 134 1512–1518 (2014).

20. Whittaker, J. R. An analysis of melanogenesis in differentiating pigment cells of ascidian embryos. *Dev. Biol.* **14**, 1–39 (1966).

21. Sarna, M., Krzykawska-Serda, M., Jakubowska, M., Zadlo, A. & Urbanska, K. Melanin presence inhibits melanoma cell spread in mice in a unique mechanical fashion. *Sci. Rep.* **9**, 1–9 (2019).

22. Pinner, S. *et al.* Intravital imaging reveals transient changes in pigment production and Brn2 expression during metastatic melanoma dissemination. *Cancer Res.* **69**, 7969–7977 (2009).

23. Yang, W. S. *et al.* Regulation of ferroptotic cancer cell death by GPX4. *Cell* **156**, 317–331 (2014).

24. Imai, H., Matsuoka, M., Kumagai, T., Sakamoto, T. & Koumura, T. Lipid peroxidation-dependent cell death regulated by GPx4 and ferroptosis. in *Current Topics in Microbiology and Immunology* vol. 403 143–170 (Springer Verlag, 2017).

25. Yang, W. S. *et al.* Peroxidation of polyunsaturated fatty acids by lipoxygenases drives ferroptosis. *Proc. Natl. Acad. Sci. U. S. A.* **113**, E4966–E4975 (2016).

26. Yagoda, N. *et al.* RAS-RAF-MEK-dependent oxidative cell death involving voltage-dependent anion channels. *Nature* **447**, 864–868 (2007).

27. Dolma, S., Lessnick, S. L., Hahn, W. C. & Stockwell, B. R. Identification of genotype-selective antitumor agents using synthetic lethal chemical screening in engineered human tumor cells. *Cancer Cell* **3**, 285–296 (2003).

28. Riegman, M. *et al.* Ferroptosis occurs through an osmotic mechanism and propagates independently of cell rupture. *Nat. Cell Biol. 2020 229* **22**, 1042–1048 (2020).

29. Yan, B. *et al.* Membrane Damage during Ferroptosis Is Caused by Oxidation of Phospholipids Catalyzed by the Oxidoreductases POR and CYB5R1. *Mol. Cell* **81**, 355-369.e10 (2021).

30. Xie, Y. *et al.* Ferroptosis: Process and function. *Cell Death and Differentiation* vol. 23 369–379 (2016).

31. Rinner, B. *et al.* MUG-Mel2, a novel highly pigmented and well characterized NRAS mutated human melanoma cell line. *Sci. Rep.* **7**, (2017).

32. Hosoi, J., Abe, E., Suda, T. & Kuroki2, T. Regulation of Melanin Synthesis of B16 Mouse Melanoma Cells by 1a,25- Dihydroxyvitamin D3 and Retinoic Acid1. *CANCER Res.* **45**, 1474–1478 (1985).

33. Heitzer, E. *et al.* Human melanoma brain metastases cell line MUG-Mel1, isolated clones and their detailed characterization. *Sci. Rep.* **9**, 4096 (2019).

34. Kemper, K. *et al.* BRAFV600E Kinase Domain Duplication Identified in Therapy-Refractory Melanoma Patient-Derived Xenografts. *Cell Rep.* **16**, 263–277 (2016).

35. JM, U. *et al.* Lymph protects metastasizing melanoma cells from ferroptosis. *Nature* **585**, 113–118 (2020).

36. Brozyna, A. A., Józwicki, W., Roszkowski, K., Filipiak, J. & Slominski, A. T. Melanin content in melanoma metastases affects the outcome of radiotherapy. *Oncotarget* **7**, 17844–17853 (2016).

37. Yang, W. S. & Stockwell, B. R. Synthetic Lethal Screening Identifies Compounds Activating Iron-Dependent, Nonapoptotic Cell Death in Oncogenic-RAS-Harboring Cancer Cells. *Chem. Biol.* **15**, 234–245 (2008).

38. J, N. *et al.* Proteomics analysis of A375 human malignant melanoma cells in response to arbutin treatment. *Biochim. Biophys. Acta* **1794**, 159–167 (2009).

39. Lange, M. J. de *et al.* Heterogeneity revealed by integrated genomic analysis uncovers a molecular switch in malignant uveal melanoma. *Oncotarget* **6**, 37824–37835 (2015).

40. Robertson, A. G. *et al.* Integrative Analysis Identifies Four Molecular and Clinical Subsets in Uveal Melanoma. *Cancer Cell* **32**, 204-220.e15 (2017).

41. Weinstein, J. N. *et al.* The cancer genome atlas pan-cancer analysis project. *Nature Genetics* vol. 45 1113–1120 (2013).

42. Tang, Z. *et al.* GEPIA: A web server for cancer and normal gene expression profiling and interactive analyses. *Nucleic Acids Res.* **45**, W98–W102 (2017).

43. G, N., H, W., D, von der H. & G, A. Establishment of two cell lines derived from conjunctival melanomas. *Exp. Eye Res.* **81**, 361–362 (2005).

44. Chen, P. W. *et al.* Expression of MAGE genes in ocular melanoma during progression from primary to metastatic disease. *Clin. Exp. Metastasis* **15**, 509–518 (1997).

45. Amirouchene-Angelozzi, N. *et al.* Establishment of novel cell lines recapitulating the genetic landscape of uveal melanoma and preclinical validation of mTOR as a therapeutic target. *Mol. Oncol.* **8**, 1508–1520 (2014).

46. Ortho- and Ectopic Zebrafish Xeno-Engraftment of Ocular Melanoma to Recapitulate Primary Tumor and Experimental Metastasis Development | Protocol.

https://www.jove.com/de/t/62356/ortho-ectopic-zebrafish-xeno-engraftment-ocular-melanoma-to.

47. Karlsson, J., Von Hofsten, J. & Olsson, P. E. Generating transparent zebrafish: A refined method to improve detection of gene expression during embryonic development. *Mar. Biotechnol.* **3**, 522–527 (2001).

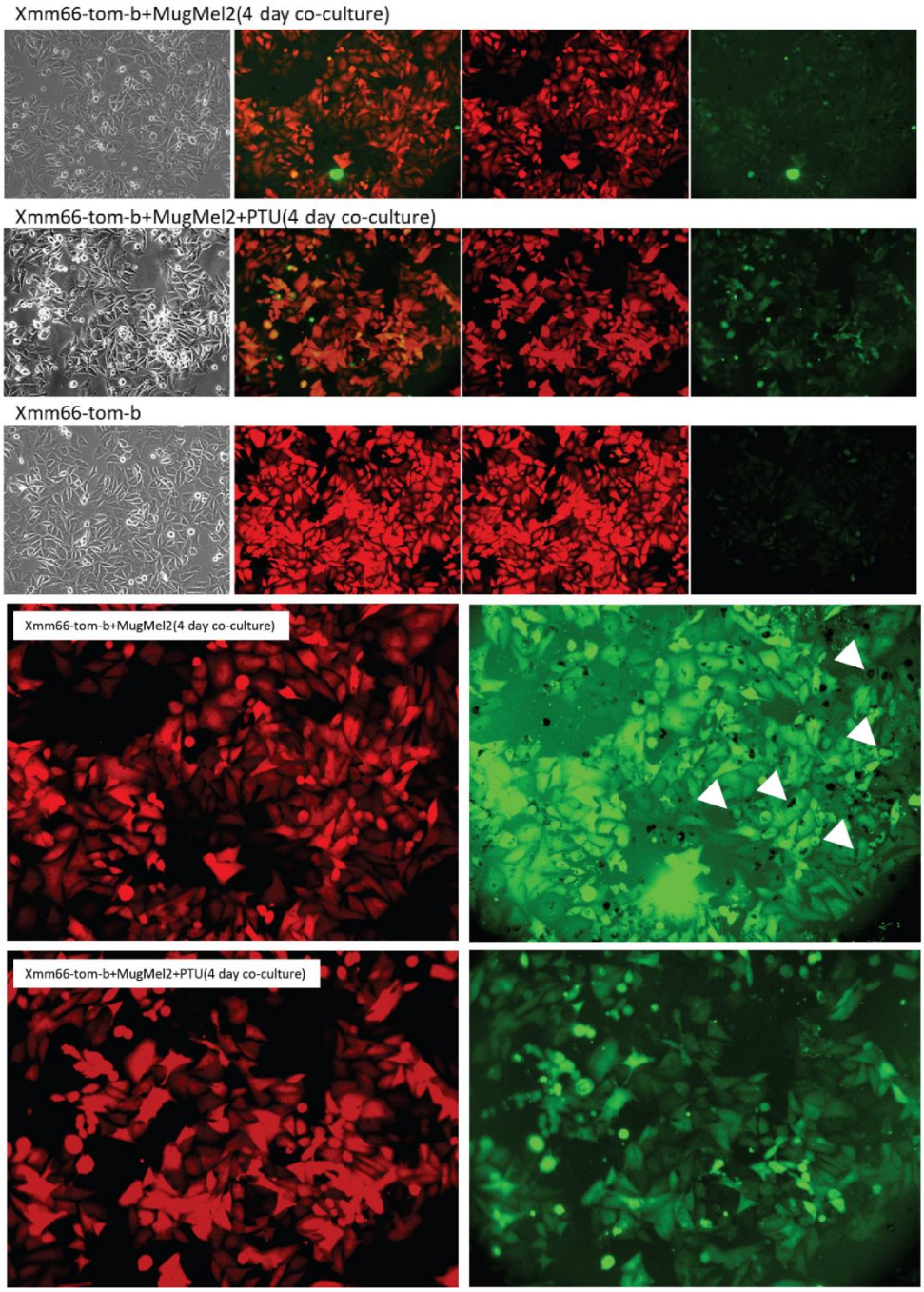

Supplementary figure S1 Co-culture of human CM melanoma cells mugmel2 and human UM cells XMM66. Example of co-cultured UM cell line XMM66 (acceptor) with melanin proficient (mugmel2 mel+) and melanin deficient (mugmel2 mel-) donor cells after mitomycin-C treatment, and control XMM66 cells. Melanin granules are present and visible in XMM66 after 4 days of co-culture (noted by the white arrowheads).

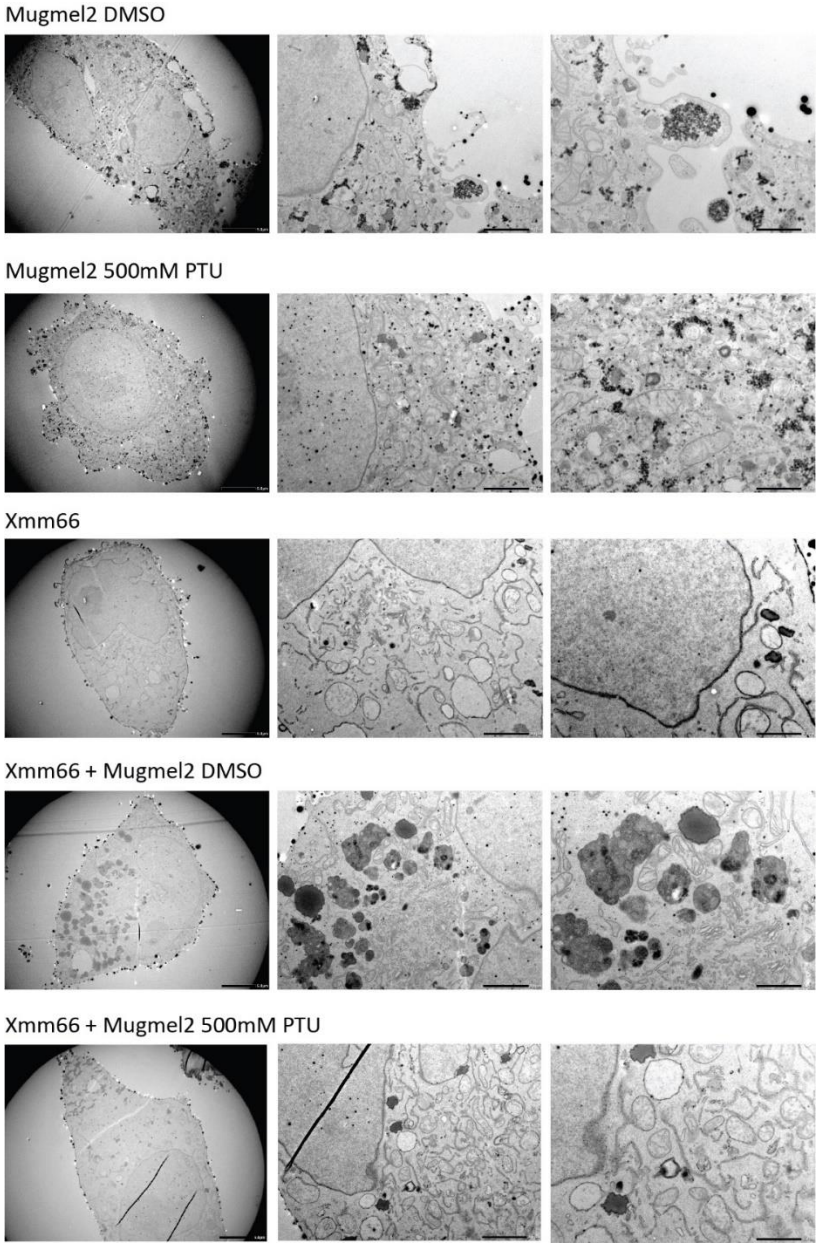

Supplementary figure S2 Transmission electron micrographs (TEM) of mugmel2 and XMM66 both with or without melanin. Mugmel2 without and with chemical melanin depletion. XMM66 naïve, melanin (mugmel2 mel+) proficient co-culture and melanin deficient (mel-) co-culture. Scalebar depicts 2µM.

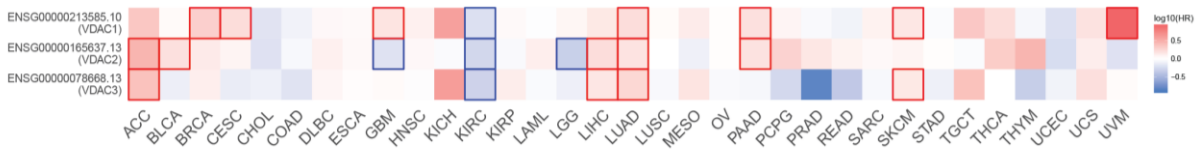

Supplementary figure S3 TCGA wide survival analysis of VDAC 1-3. Comparative analysis of all TCGA datasets for VDAC1-3. Red bounding boxes indicate a significant negative correlation between gene expression and survival. VDAC1 expression correlates with a decreased overall survival in breast, cervical squamous cell carcinoma and endocervical adenocarcinoma, glioblastoma multiforme, lung-, pancreatic adenocarcinoma, skin cutaneous and uveal melanoma (21.2% of all TCGA data sets).

TCGA abbreviations: Adrenocortical carcinoma (ACCA), Bladder Urothelial Carcinoma (BLCA), Breast invasive carcinoma (BRCA), Cervical squamous cell carcinoma and endocervical adenocarcinoma (CESC) Cholangio carcinoma (CHOL), Colon adenocarcinoma (COAD), Lymphoid Neoplasm Diffuse Large B-cell Lymphoma (DLBC), Esophageal carcinoma (ESCA), Glioblastoma multiforme (GBM), Head and Neck squamous cell carcinoma (HNSC), Kidney Chromophobe (KICH), Kidney renal clear cell carcinoma (KIRC), Kidney renal papillary cell carcinoma (KIRP) Acute Myeloid Leukemia (LAML) Brain Lower Grade Glioma (LGG), Liver hepatocellular carcinoma (LIHC), Lung adenocarcinoma (LUAD), Lung squamous cell carcinoma (LUSC), Mesothelioma (MESO), Ovarian serous cystadenocarcinoma (OVO), Pancreatic adenocarcinoma (PAAD), Pheochromocytoma and Paraganglioma (PCPG), Prostate adenocarcinoma (PRAD), Rectum adenocarcinoma (READ), Sarcoma (SARC), Skin Cutaneous Melanoma (SKCM), Stomach adenocarcinoma (STAD), Testicular Germ Cell Tumors(TGCT), Thyroid carcinoma (THCA), Thymoma (THYM), Uterine Corpus Endometrial Carcinoma (UCEC), Uterine Carcinosarcoma (UCSU), Uveal Melanoma (UVM).